J Mater Sci (2010) 45:4906–4911
DOI 10.1007/s10853-010-4271-4

ICAM 2009

High-density gas aggregation nanoparticle gun applied to the production of SmCo clusters

G. T. Landi · A. D. Santos

Received: 5 October 2009 / Accepted: 26 January 2010 / Published online: 9 February 2010

Abstract We describe in this article the application of a high-density gas aggregation nanoparticle gun to the production and characterization of high anisotropy SmCo nanoparticles. We give a detailed description of the simple but efficient experimental apparatus with a focus on the microscopic processes of the gas aggregation technique. Using high values of gas flux (~45 sccm) we are able to operate in regimes of high collimation of material. In this regime, as we explain in terms of a phenomenological model, the power applied to the sputtering target becomes the main variable to change the size of the clusters. Also presented are the morphological, structural, and magnetic characterizations of SmCo nanoparticles produced using 10 and 50 W of sputtering power. These values resulted in mean sizes of ~12 and ~20 nm. Significant differences are seen in the structural and magnetic properties of the samples with the 50 W sample showing a largely enhanced crystalline structure and magnetic anisotropy.

Introduction

In recent years, the production and characterization of nanoparticles (NPs) made of different materials has become of vast interest to the scientific community, especially due to the novel properties observed in such systems. Ranging from optical [1], electronic [2], and magnetic [3], these properties are often related to surface interaction phenomena and may be observed when studying not only the NPs [4] but also their interaction with a matrix in which they are embedded [5].

Several techniques have been developed to produce nanoparticles, but only some of them accept matrix co-deposition [6]. The gas aggregation method [7], which relies on a physical vapor deposition system such as a magnetron sputtering, is usually a good solution to this issue. In our case, it consists of an adaptation in one of the sputtering guns to support a high-pressure auxiliary condensation chamber. Inside it, the thermalized atomic vapor condenses into NPs through collisions with neighboring specimens.

In terms of technological applications, the production of magnetically hard NPs made from alloys such as SmCo [8], FePt, and CoPt [9], is of vast interest. These may be used in ultra-high density magnetic recording media, which requires diminishing grain sizes to minimize the signal-to-noise ratio [10]. Also, through exchange coupling of magnetic phases, embedding these magnetically hard, high coercivity clusters on a magnetically soft matrix with high saturation magnetization may lead to enhanced exchange-spring nano-composites [11]. Such systems may have magnetic properties that are superior to that of a single phase magnet and are of interest in the field of permanent magnets.

Generally, in the gas aggregation methodology, there are no restrictions as to the final thickness of the sample. But unfortunately for many applications, including the ones just described, long deposition times would be necessary to achieve the desired thickness [12].

Therefore, the purpose of this work is two-fold. In terms of experimental setup, we will describe a cluster gun whose methodology is based on a variation of the gas aggregation method. Unlike other systems, with it we are able to obtain high deposition rates while still maintaining relatively good

G. T. Landi (✉) · A. D. Santos
Laboratório de Materiais Magnéticos, Departamento de Física dos Materiais e Mecânica, Instituto de Física da Universidade de São Paulo, Caixa Postal 66318, 05314-970 São Paulo, SP, Brazil
e-mail: gtlandi@if.usp.br

size control and dispersion. Afterwards, in terms of experimental results, we will present the production and characterization of high anisotropy SmCo NPs of two distinct sizes: $\sim$12 and $\sim$20 nm. Strong differences have been observed on the crystallographic and magnetic properties of each size.

Experimental setup

The cluster gun (Fig. 1) was constructed as an adaptation to one of the guns of a 4-gun commercial magnetron sputtering system (AJA 2000 International, 2 inches gun). It consists of a 10 cm wide by 15 cm long cylindrical chamber sealed around the sputtering target. A high Ar flux of around 45 sccm is injected near the target and directed onto the only aperture of the chamber, which is 2 mm wide and located on its opposite end. The chamber outside the aperture operates at standard sputtering pressures of $\sim$3 mTorr. Inside the condensation chamber, a flux of 45 sccm results in a pressure of about 600 mTorr. The sputtering gun is water cooled, and the condensation chamber operates at ambient temperature.

Inside the cluster gun, the sputtered atomic vapor is removed from the target with energies of the order of a few eV. After being removed, they will thermalize very quickly in a region still very close to the target. This is mainly because the Ar mean free path is around a few microns and only 5–10 collisions are enough to reduce the vapor's energy to the order of the gas kinetic energy ($\sim 10^{-1}$ eV) [13]. After thermalizing, the sputtered material will follow the gas lamellar trajectory inside the condensation chamber on the way to the aperture. Along this path, through collisions with neighboring specimens, the vapor will gradually condense into clusters. The condensation does not occur only through the aggregation of atoms to an already nucleated particle but especially through the agglomeration between particles. Since this occurs in a low-energy environment, it is expected that the as-produced NPs will consist of multiple grains.

The main aspect that stands out in this system is that almost all the sputtered material is collimated into the lamellar Ar flow during the condensation process inside the condensation chamber. This occurs whenever the number of Ar atoms is sufficiently larger than the number of sputtered atoms. The phenomenology behind this is that the gas must thermalize the vapor before it starts condensing. Otherwise, even though the sputtered atoms will still condense into NPs, these will not follow the gas trajectory but instead will become fixed on the inner walls of the chamber. For SmCo, the high collimation, which is of great interest to us, happens in the range between 30 and 100 sccm. Below 30, the number of Ar atoms is no longer enough to quickly thermalize the atomic vapor. On the other hand, fluxes above 100 sccm create turbulent states in the regions near the aperture also debilitating the collimation. The relationship between the collimation capability and the flux is highly nonlinear with 30 sccm being a visible threshold in the deposition of material.

The flow or Ar + NPs, after passing through the aperture, will expand outwards aerodynamically. The NPs are then collected on the substrates placed $\sim$3 cm away from the chamber. The material deposited forms a circular dark stain with $\sim$3 mm of diameter. The deposition has the form of a Gaussian distribution of material with the center having considerably more material than for a regular sputtering deposition. Much like any sputtering system, there is no restriction as to the substrate used. Since the substrate-holder is located outside the condensation chamber, we are also able to use the other guns to either embed the NPs in dielectric, metallic, or multilayer matrixes or to just cover them with a capping layer for chemical protection. Finally, the substrate-holder may rotate around its axis. This dilutes the circular stain of NPs into a circular ring, which has two effects. First, the deposition rates can be reduced at least one order of magnitude and become comparable with regular sputtering depositions, which is useful for matrix embedding. Second, several identical samples can be produced simultaneously over the ring, each using a different substrate.

For the actual configuration, the Ar flux and the sputtering power are the available parameters to control the size of the clusters. But, it has been experimentally

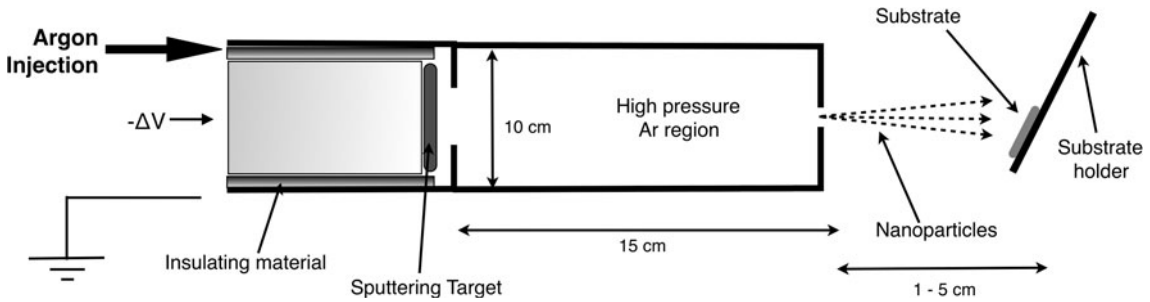

Fig. 1 Schematic view of the cluster gun constructed on top of a sputtering gun

observed that varying the flux has no influence on the size. As long as the number of Ar atoms remains high, compared to the sputtered vapor, no changes can be observed in the size of the particles as a function of the gas flow. Therefore, the role of the Ar gas while in the high collimation regime is merely thermalizing the atomic vapor and carrying the specimens during the condensation process inside the condensation chamber. Below 30 sccm or above 100 sccm, when outside of the high collimation regime, there is no solid information about the dependence of the particle size with the flux.

On the other hand, the power applied to the gun (P) linearly determines the number of atoms being removed from the target. If we assume that all atoms inside the condensation chamber condense into nanoparticles, a result corroborated by electron microscopy, then P will directly affect the number of atoms in each cluster (n). Furthermore the diameter of the particle (D) is proportional to $n^{1/3}$, which finally leads us to $D \propto P^{1/3}$. This corresponds to a phenomenological relationship between the power applied to the target and the final mean diameter of the NPs as long as the flux is between 30 and 100 sccm. For example, a 5-fold increase in power leads to a $\sim$1.7-fold increase in size.

The cost of the adaptation of the multiuser sputtering system to the gas aggregation condensation chamber is negligible. The installation takes only a couple of hours, and it is almost as simple to operate as the sputtering itself.

Four samples have been produced using a $SmCo_5$ sputtering target. The first three samples were prepared using 45 sccm of Ar flux and 10 W of power. For analysis with transmission electron microscopy (TEM), a Cu grid coated with a polymeric layer and a carbon thin film was used. The NPs were deposited on top of the grid for 5 min with the substrate-holder rotating (sample S1). For scanning electron microscopy (SEM) a similar sample was made but on a Si substrate (sample S2). The third 10 W sample, S3, also used Si but had 20 min of deposition time and the substrate-holder static. Finally, for sample S4, we maintained 45 sccm of Ar flux and used 50 W of power. The deposition time was 10 min also on Si. Samples S3 and S4 were both produced co-depositing Si_3N_4 (100 W RF) and with a magnet placed under the substrates producing a magnetic field perpendicular to them. X ray diffraction (XRD) and vibrating sample magnetometry (VSM) measurements were performed on both.

Sample characterization

Figure 2 depicts two high resolution transmission electron microscopy (TEM) images of sample S1 (10 W). The small amount of material seen on Fig. 2a is compatible with the small deposition time and the rotation of the substrate-holder. The mean sizes are around 12 nm. An accurate size distribution histogram was not easily obtained because of the high NP–NP aggregation. As discussed in the previous section, the process of production of the NPs is itself an agglomeration of smaller clusters. Also, the magnetic behavior of the SmCo alloy enhances the NP–NP aggregation and deflects the electron beam blurring the image. Even still, one may conclude from analyzing the image that the particle's sizes have a relative dispersion (FWHM) no higher than 30%. Similar studies using our system, but for Co NPs, have shown a 14% dispersion in a lognormal distribution [14]. Figure 2b depicts a magnification of 12-nm particles. No crystallographic planes can be observed.

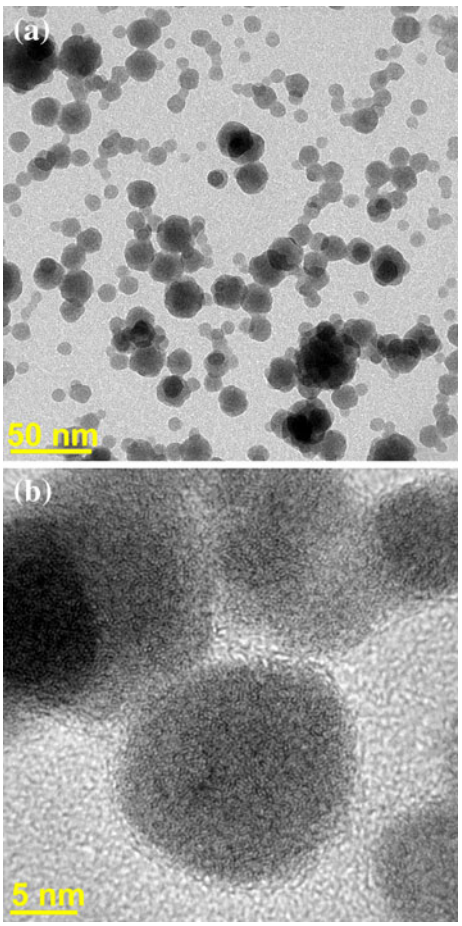

Fig. 2 TEM images of sample S1 produced using 10 W of power and 45 sccm of Ar flux. This sample was produced in 5 min with the substrate holder rotating in order to obtain a sample with dispersed particles. Strong NP–NP coupling can be observed as well as the absence of crystallographic planes

Scanning electron microscopy (SEM) images of samples S2 and S3 are shown in Fig. 3. Sample S2 was prepared with 5 min of deposition and with the substrate-holder rotating. For sample S3, the substrate-holder was still and the total deposition time was 20 min. The considerable

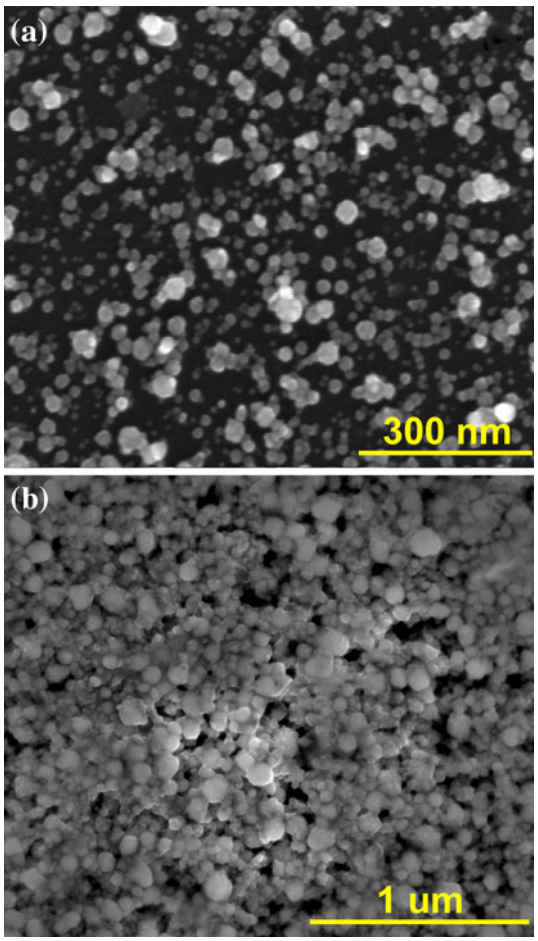

Fig. 3 SEM images of samples **a** S2 and **b** S3. Both were produced on the same conditions but sample S3 was produced with four times more time and with the substrate holder still. The strong differences in the amount of material are observed

difference in the amount of material from one sample to the other can be clearly observed in these images. Due to the enhanced magnetic properties of the NPs, the samples are highly porous and have a low packing factor. Care was taken when choosing the position where the images were taken so they all were on top of the Gaussian distribution of material (discussed on the previous section).

Auxiliary measurements by Rutherford back-scattering indicate that the deposition rates observed on the middle of the distribution corresponds to a 500-fold increase if compared to a regular sputtering deposition of SmCo with 5 mTorr of pressure and 10 W of power. The half-height width of the distribution of material is around 2 mm. This means that the high deposition rates are much localized. On the other hand, the sputter yield (number of atoms removed per Ar ion) of a material is greatly reduced in high pressures. For 600 mTorr, this corresponds to approximately a 100-fold reduction if compared to 5 mTorr usual sputtering depositions. Finally, we observe that there is no material

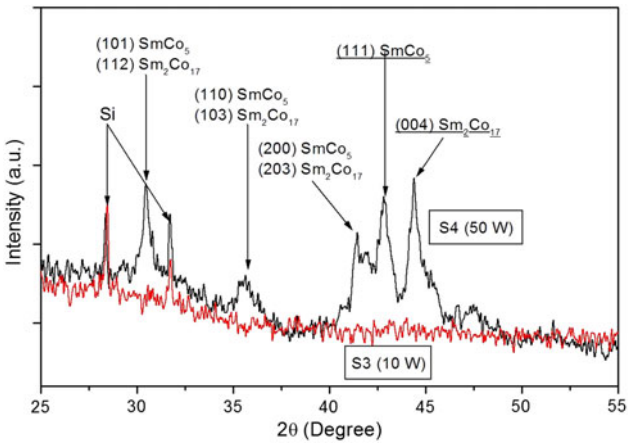

Fig. 4 XRD measurements of samples S3 (10 W) and S4 (50 W) denoting the crystallographic peaks of each phase. The peaks corresponding to the Si substrate are also shown. As can be observed, the 10 W sample does not present any clear crystallographic texture. The 50 W sample, on the other hand, shows enhanced peaks corresponding to mixed $SmCo_5$ and Sm_2Co_{17} phases

deposited on the inner walls of the condensation chamber, even after hours of operation. This means that almost all the material effectively removed from the target is condensed into NPs, removed from the condensation chamber and deposited on the substrate. Therefore, the enhanced deposition rates correspond not to an increase in sputtered material, but to a strong collimation of a reduced amount of atoms.

Figure 4 illustrates diffractograms of samples S3 and S4. Some of the peaks that appear in both correspond to the Si substrate, as denoted on the figure. The absence of peaks for sample S3 (10 W) indicates that the grain sizes are small. A very different result is obtained for sample S4 (50 W) where large crystallographic peaks are observed. Comparing with SmCo diffraction peaks in the literature, the stronger lines correspond to both hexagonal $SmCo_5$ [15] and Sm_2Co_{17} [16] phases. The only exceptions are the 42.8 and 44.4° peaks which correspond exclusively to $SmCo_5$ (111) and Sm_2Co_{17} (004), respectively. This mixing of phases is characteristic of this alloy. The enhancements in the crystallographic texture between samples S3 and S4 may possibly be associated with the higher temperature during the condensation process due to the higher power applied. Using Scherrer's formula, we estimate the mean size of the crystallographic grains in sample S4 as $\sim$20 nm. This size is compatible with the $P^{1/3}$ phenomenological model described in "Experimental setup" section.

Hysteresis loops for samples S3 (10 W) and S4 (50 W), in and out of plane, are shown in Fig. 5. On all four measurements, the paramagnetic behavior of the Si substrate was subtracted. From the data it can be seen that both

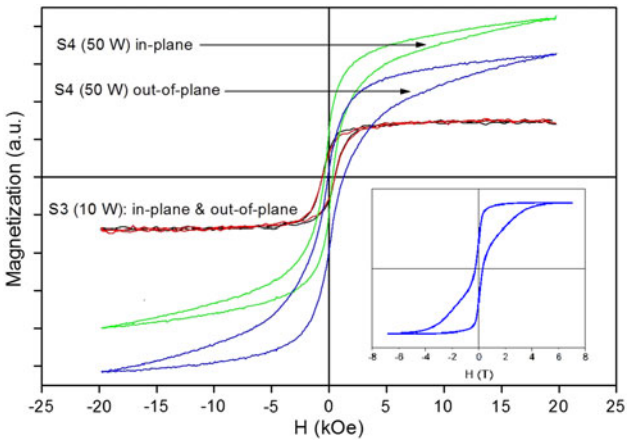

Fig. 5 In-plane and out-of-plane hysteresis loops of samples S3 (10 W) and S4 (50 W). The clear differences in moment and anisotropy can be observed. The applied 2 T field was not enough to saturate the 50 W sample. The inset shows the out-of-plane SQUID measurement of the 50 W sample indicating that 4 T was necessary to saturate it. The measured coercive field is 3 kOe

samples are, as expected, ferromagnetic. For sample S3 (10), the measured coercivity is around 550 Oe. The absence of preferential axes of magnetization is observed with both in-plane and out-of-plane curves being very similar. This result was expected since materials with low crystallographic texture do not show preferential axes of magnetization.

Sample S4, on the other hand, shows a very different behavior. For both the in-plane and out-of-plane measurements, the 2 T field was not enough to saturate the sample. The out-of-plane curve is also shifted downwards indicating a strong remanence. Therefore, the coercivity of this sample cannot be correctly measured on these curves. In order to better study the coercivity, out-of-plane SQUID measurements were performed on sample S4. The results are shown on the inset of Fig. 5. The measured coercive field is 3 kOe. This represents a significant increase in coercivity if compared to the other sample. This change in the magnetic behavior, from one sample to the other, likely has been directly influenced by the changes in crystallographic texture shown in Fig. 4. Finally, it is unviable to measure the total mass of the samples in order to determine their actual magnetic moment. But, even still, it can be seen on Fig. 5 that sample S4 has around four times more moment than sample S3.

Conclusions

We described in this article the application of a nanoparticle gun constructed as a simple and cheap adaptation to a multipurpose magnetron sputtering systems. With this system we are able to produce NPs from a broad range of materials and embed them on dielectric, metallic, or multilayer matrixes. Using specific values of Ar flux, we are able to operate on regimes of high collimation of material. This technique significantly decreases the deposition times required to obtain thick samples while still maintaining good size control.

We presented the production and characterization of SmCo NPs in two distinct conditions: 10 and 50 W. We verified experimentally that these values resulted in particles with $\sim$12 and $\sim$20 nm of diameter. This is consistent with the $P^{1/3}$ model also discussed. Due to the enhanced magnetic properties of the SmCo alloy, a strong coupling between NPs was observed, which resulted in samples with high porosity and a low packing factor. We were only able to observe crystallographic peaks on the 50 W samples. These corresponded to a mixed $SmCo_5$ and Sm_2Co_{17} phases. All samples presented a ferromagnetic behavior. The 50 W sample showed a significant increase in anisotropy. The applied 2 T field was not enough to fully saturate both in-plane and out-of-plane curves. The out-of-plane presented a shifted loop showing a strong remanence, likely related to the application of a magnetic field perpendicular to the sample during the preparation process. Further measurements using stronger fields indicated that 4 T was necessary to saturate this sample, which then presented a coercive field of 3 kOe.

Acknowledgements This study was supported by the Brazilian funding agencies, Fundação de Ampáro a Pesquisa do Estado de São Paulo (FAPESP), and the Conselho Nacional de Desenvolvimento Científico e Tecnológico (CNPq). The authors thank Professor M.C. Fantini for the x ray diffraction measurements, and the Centro de Ciência e Tecnologia dos Materiais (CCTM-IPEN) for the TEM images.

References

1. de Heer WA (1993) Rev Mod Phys 65:611
2. Berkowitz AE, Mitchell JR, Carey MJ, Young AP, Zhang S, Spada FE, Parker FT, Hütten A, Thomas G (1992) Phys Rev Lett 68:3745
3. Bansmann J, Baker SH, Binns C, Blackman JA, Bucher J-P, Dorantes-Dávila J, Dupuis V, Favre L, Kechrakos D, Kleibert A, Meiwes-Broer K-H, Pastor GM, Perez A, Toulemonde O, Trohidou KN, Tuaillon J, Xie Y (2005) Surf Sci Rep 56:189
4. Gabardella P, Rusponi S, Veronese M, Dhesi SS, Grazioli C, Dallmeyer A, Cabria I, Zeller R, Dederichs PH, Kern K, Carbone C, Brune H (2003) Science 300:1130
5. Iakaubovskii K, Mitsuishi K (2008) Phys Rev B 78:064105
6. Hyeon T (2003) Chem Commun 8:927
7. Mühlbach J, Recknagel E, Sattler K (1980) Surf Sci 106:188
8. Chinnasamy CN, HUang JY, Lewis LH, Latha B, Vottoria C, Harris VG (2008) Appl Phys Lett 93:032505
9. Sun S, Murray CB, Weller D, Folks L, Moser A (2000) Science 287:1989
10. Moser A, Takano K, Margulies DT, Albrecht M, Sonobe Y, Ikeda Y, Sun S, Fullerton EE (2002) J Phys D Appl Phys 35:157

11. Kneller EF (1991) IEE Trans Mag 27:3588
12. Baker SH, Thornton SC, Edmonds KW, Maher MJ, Norris C, Binns C (2000) Rev Sci Inst 71:3178
13. Stirling AJ, Westwood WD (1971) J Phys D Appl Phys 4:246
14. Landi GT, Romero SA, Santos AD (2009) Rev Sci Instrum (submitted)
15. JCPDS (1995) International centre of diffraction data, pp 35–1400
16. JCPDS (1995) International centre of diffraction data, pp 35–1368